DOI: 10.1002/adma.((please add manuscript number))

Author Manuscript

In-situ Nanoscale Electric Field Control of Magnetism by Nanoionics

Xiaojian Zhu[1], *Jiantao Zhou*[1], *Lin Chen*[1], *Shanshan Guo*[2], *Gang Liu*[2], *Run-Wei Li*[2], *and Wei D. Lu*[1]*

Dr. X. Zhu, J. Zhou, Dr. L. Chen, Prof. W. D. Lu

Department of Electrical Engineering and Computer Science, the University of Michigan, Ann Arbor, Michigan 48109, USA

S. Guo, Dr. G. Liu, Prof. R.-W. Li

Key Laboratory of Magnetic Materials and Devices, Ningbo Institute of Materials Technology and Engineering, Chinese Academy of Sciences, Ningbo, Zhejiang 315201, China

E-mail: wluee@eecs.umich.edu

Keywords: Nanomagnetism, ion migration, resistive switching, intensity of the magnetization, domain wall

This is the author manuscript accepted for publication and has undergone full peer review but has not been through the copyediting, typesetting, pagination and proofreading process, which may lead to differences between this version and the Version of Record. Please cite this article as doi: 10.1002/adma.201601425.

This article is protected by copyright. All rights reserved.

Electric field control of ion migration in semiconductors can introduce desired changes in the material's stoichiometry, defect profile and lattice structure, which in turn offers a versatile and convenient means to modify the materials' chemical compositions and physical properties at the nanoscale and *in-situ.*[1,2] This field, termed nanoionics, has emerged as a new discipline that promotes the development of new materials and devices towards a broad range of electronic and energy applications.[3,4] For example, in a two-terminal metal/insulator/metal structure, the electric field induced ion migration and the associated redox processes can lead to changes in local conductivity and an overall change in the structure resistance, resulting in resistive switching (RS) effects.[5-7] The ion migration induced RS effects can originate from the migration and redistribution of cations (*e.g.* Ag^{+} or Cu^{2+} ions) or anions (*e.g.* O^{2-} ions), and detailed experimental studies[8,9] and theoretical analyses[10,11] have been carried out to reveal the dynamic ion migration processes and obtain (semi-)quantitative information (*e.g.* ion diffusion energy barrier) of the ion migration process *in-situ* at the nanoscale. Recent studies have also suggested that the controlled ion migration can modulate the materials' optical properties,[12] extending the range of nanoionics beyond RS effects. Nanoioncs has also been widely studied in the energy conversion/storage fields and leads to various advanced battery applications.[13]

Electric control of magnetism at the nanoscale holds great potential in reducing power consumption and increasing device density in spin-based memory and logic systems.[14-18] So far, electric field control of magnetism has been demonstrated through the modulations of charge carrier concentrations in ferromagnetic semiconductors,[19,20] electron orbital occupancy in ultrathin ferromagnetic metals[21,22] and magnetoelectric coupling effects in

Author Manuscript

This article is protected by copyright. All rights reserved.

multiferroics[23-28], leading to promsing device applications[29-31]. However, most of these effects are either volatile or indirect/weak. It has been demonstrated very recently that by controlling the migration and redistribution of cations (Li^+ or Co^{2+} ions) or anions (O^{2-} ions), it is possible to control the material's magnetic moment and magnetic anisotropy.[32-34] These studies presented initial, promising examples of ion migration induced magnetism control, although how the nanoscale, local magnetic properties are affected by ion migration still remain unclear. Here, we report experimental studies on *in-situ* modulation of nanocale magnetic domains in lithium ferrite thin films, which clearly reveal the dynamic evolution of individual domains and the motion of domain walls during the ion migration process. We show that the de-intercalation/intercalation of Li^+ ions not only leads to RS effects, but also directly affects the chemical states of iron ions. By studying the evolution of individual magnetic domains during ion migration, we find that the intensity of the domains' magnetization can be reversibly modulated by ~100% and observe domain wall motion over 100 nm, accompanied by RS effects between a high resistance state (HRS) and a low resistance state (LRS). Finally, we show that the Li^+ ions driven magnetism changes can lead to reliable, fast and multilevel data storage elements, through the local control of magnetization direction and intensity of individual magnetic domains.

Inverse spinel structured lithium ferrite ($LiFe_5O_8$) was selected for our study due to the low activation energies for Li^+ ion migration in lithium ferrite[35] and the hypothesis that the redox processes associated with Li^+ ion de-intercalation/intercalation can possibly modulate the iron ion's chemical states and thus the material's magnetic properties. In $LiFe_5O_8$, the Li^+ ions and three-fifths of the Fe^{3+} ions occupy the center of the octahedral sites (referred to as

Author Manuscript

This article is protected by copyright. All rights reserved.

the B sites) while the rest of the Fe^{3+} ions occupy the center of the tetrahedral sites (referred to as the A sites) (**Figure 1**a).[36,37] The Fe^{3+} ions at A and B sites are antiferromagnetically coupled and the net magnetic moment is determined by the difference of the A and B-site occupied ions. For example, in oxygen-deficient lithium ferrite $LiFe_5O_{8-x}$ (LFO)[38] some of the B site Fe^{3+} ions with magnetic moment 5 μ_B (μ_B: Bohr magneton) can be reduced to Fe^{2+} ions with magnetic moment 4 μ_B,[32] thus leading to an overall lower magnetic moment. During Li^+ ions de-intercalation, the B-site Fe^{2+} ions can be oxidized to Fe^{3+} ions again hence increasing the magnetic moment correspondingly (Figure S1, Supporting Information). The reverse process occurs during Li^+ ions intercalation. As a result, we expect electric-field controlled Li^+ ion de-intercalation/intercalation can lead to reversible and direct modulation of the film's magnetization. In the meantime, the Li^+ ion de-intercalation/intercalation process modulates the local concentration of hopping centers such as Li^+ vacancies in the film, which in turn can lead to RS effects and provides a convenient means to observe and analyze the ionic processes.

Magnetic and electrical measurements were performed on devices based on a Pt (60 nm)/LFO(25 nm)/$SrRuO_3$ (SRO, 60 nm) structure where the Pt and SRO layers serve as top and bottom electrodes, and the active device area is defined by a via structure (see Methods and Figure S2, Supporting Information). X-ray diffraction (XRD) studies (Figure S3, Supporting Information) suggest that the LFO film is (111) orientated,[38] with the out-of-plane direction along the magnetocrystalline easy axis.[36] X-ray photoelectron spectroscopy (XPS) results (Figure S4, Supporting Information) indicate the existence of Fe^{2+} ions in the virgin (as-deposited) LFO film. The Magnetic Force Microscopy (MFM) technique was used to investigate the evolution of magnetic

Author Manuscript

This article is protected by copyright. All rights reserved.

domain properties during the ion migration processes. The schematic of the setup during the measurement is illustrated in Figure 1b.

Under an applied electric field, the devices were found to show stable bipolar RS behaviors. Typical current-voltage (*I-V*) curves during RS are shown in Figure 1c. The device at the virgin state (VS) was highly insulating with a resistance of 4×10^6 Ω measured at 0.1 V. During a positive bias voltage sweep process, the Pt/LFO/SRO device was switched to a LRS with a resistance of ~200 Ω under a compliance current of 3 mA. This first switching process is termed as the Forming process. Subsequently, negative and positive voltage sweeps were found to alternatively switch the device between a LRS (~200 Ω) and a HRS (~3×10^3 Ω), respectively. Changes of the device resistance during these RS processes are shown in Figure 1d. These different resistance states are nonvolatile and stable for weeks without obvious degradation. Interestingly, we observed that accompanying the RS processes, the magnetization of the magnetic domains in the LFO film was reversibly changed as well. Figure 1e shows the corresponding morphology and MFM images of the device at different resistance states. The MFM image at VS (①) shows the initial magnetic domain structure of the LFO thin film beneath the Pt electrode, where the red and green areas correspond to magnetic domains with upward and downward magnetization directions, respectively. After the Forming process that switched the device to the LRS, two distinguishable features in the MFM image (②) can be consistently observed in several regions: 1. the intensity of the magnetization of domains with both upward and downward directions was enhanced in general (as indicated by the increased phase values in the MFM images at positions marked by the crosses); and 2. the magnetization direction of some domains was reversed (as indicated by the reversal of phase polarity in the region marked by the circle). The fact that the magnetism modulation is local is consistent with RS effects which are driven by ion migration through localized paths, *e.g.* due to film inhomogenities.[5] This hypothesis is

This article is protected by copyright. All rights reserved.

Author Manuscript

further verified by the weak dependence of the LRS resistance on the electrode area (Figure S5, Supporting Information). It is noted that this effect is nonvolatile (Figure S6 and S7, Supporting Information) and reversible, as shown in Fig. 1e,f. Subsequent switching of the device back to the HRS correspondingly decreased the intensity of the marked domains (③), and further switching the device to the LRS caused the intensity to increase again (④), indicating that the magnetization in these domains are related to the RS effects and can be reversibly controlled by cycling the device between the HRS and the LRS (Figure 1e,f). Similar behaviors have been consistently observed in over thirty devices. These observations suggest that the magnetization of the domains in LFO films can be reversibly modulated *in-situ* by an electric field, and may originate from the same underlying atomic processes that also drive RS behaviors, thus potentially enabling the study and development of multi-functional systems based on nanoionics.

To directly correlate the nanoscale RS effects and magnetism modulation in the Pt/LFO/SRO devices, we studied the local electrical conduction characteristics of the device using a conductive AFM (CAFM) technique after the Forming process. After removing the Pt electrode of the device at the LRS (see Methods and Figure S8, Supporting Information),[39] we found that the same area where the magnetic properties have been apparently changed also became highly conductive, in contrast to the areas which showed no obvious magnetism changes and also remained insulating (Figure S9, Supporting Information). Local *I-V* measurements suggest the observed bipolar RS behaviors in the device originate from the RS effects in these local conductive regions whereas the insulating regions remain unchanged (Figure S9, Supporting Information). These results further support the concept that changes in the film's magnetic properties are due to nanoscale, local modulations, and are likely of the same origin of the local RS effects.

More detailed information on the ion-migration process can be obtained by systematic

This article is protected by copyright. All rights reserved.

Author Manuscript

studies on the RS process. Analyzing the Forming process shows that the time it takes to form the device increases exponentially with a decrease in the Forming voltage, consistent with the ion hopping model (Figure S10, Supporting Information).[5] The ion hopping distance and the hopping energy barrier can be extracted to be 0.57 nm and 0.59 eV respectively from the voltage-dependent pulse width measurements (See discussion in Supplementary Information), which are comparable to the distance between two neighboring lattice Li^+ ions (~0.5 nm) and the activation energy of Li^+ ions in similar spinel structured lithium oxides (*e.g.* ~0.52 eV in $LiMn_2O_4$[40]), again supporting the concept of Li^+ ion migration as the mechanism behind the observed magnetization modulation and RS effects[41-43]. Temperature dependence measurements of the device at both the LRS and the HRS show a thermal-activation behavior and suggesting the semiconducting nature at both states (Figure S11, Supporting Information). This behavior is different from previous observations of RS effects in $NiFe_2O_4$ ferrite films where the Ni cations are difficult to migrate and the redistribution of oxygen-vacancies leads to metallic conduction behavior at the LRS.[44] Instead, our analysis of the LFO device's *I-V* behaviors showed that the conduction of the device at both the HRS and the LRS can be well fitted by the space charge limited current (SCLC) model (Figure S12, Supporting Information),[45] suggesting a defect mediated conduction mechanism at both the HRS and the LRS. Based on these observations and the observed magnetization modulation accompanying the RS behaviors shown in Figure 1, we propose the following mechanism: during the SET process, the electric-field driven de-intercalation of Li^+ ions in the LFO layer leads to the formation of conductive channels composed of Li^+ ion vacancies. This process simultaneously oxidizes Fe^{2+} (with low spin state 4 μ_B) to Fe^{3+} (with high spin state 5 μ_B), thus resulting in the device switching into the LRS and enhancement of the magnetization;

This article is protected by copyright. All rights reserved.

Author Manuscript

the reverse processes during RESET lead to the device switching into the HRS and weakening of the magnetization in the LFO layer. During the Li de-intercalation (intercalation) process, the Li ions are likely stored in (released from) the $SrRuO_3$ ($SrO\text{-}RuO_2$)[46] electrode, which plays a similar role as RuO_2 electrodes in lithium batteries[47]. As a result, through electric-field driven Li^+ ions de-intercalation/intercalation the local magnetic properties can be reversibly tuned *in-situ*. Additionally, the accompanying RS effects offers a convenient means to control and monitor the degree of Li^+ ions migration for systematic tuning of induced magnetization changes. We note that additional systematic studies are still needed to fully reveal the filament formation processes, including the Li de-intercalation/intercalation dynamics, the stability of the filament and the Li-ion storage mechanism.

To verify this hypothesis and study the semi-quantitative relationship between the magnetization modulation and ion migration, we characterized the evolution of the magnetization of a single magnetic domain in the LFO film as the device was gradually programmed into different resistance states. The Pt/LFO/SRO device, starting from the HRS, was first switched to an intermediate resistance state (IRS) and then the LRS by increasing the SET compliance current from 1 mA to 3 mA during two successive SET processes (**Figure 2**a, processes 1 and 2). Afterwards, two successive RESET processes were used to switch the device back to the IRS and then the HRS respectively, with increasing RESET voltage from -2 V to -3 V (process 3 and 4). The resistance changes are shown in Figure 2b. Figure 2c shows the MFM images of a region in the device containing a dominant upward-magnetized domain at different resistance states. Throughout different stages of the

Author Manuscript

This article is protected by copyright. All rights reserved.

RS process, the magnetization of the domain also changed accordingly, suggesting this area to be a region where Li^+ ions migration has occurred. It was found that after each SET/RESET process, the magnetization in this region strengthened/weakened in general. However, the magnetization modulation was not uniform. For example, during process 1, the magnetization in area 1 was significantly enhanced, in contrast with that in area 2, while the opposite behavior was observed during process 2. These trends were more clearly illustrated by plotting the evolutions of the phase values for the two positions marked in areas 1 and 2 during the RS process, shown in Figure 2d. The results suggest that when switching from the HRS to the LRS, the de-intercalation of Li^+ ions initially occurs in a localized region (area 1) and correspondingly strengthens the magnetization there, continued programming in process 2 leads to an expansion of the de-intercalated region and the strengthening of magnetization in surrounding area 2. These observations are again consistent with the ion-migration model in cation- and anion-based RS devices where the filament growth can be roughly separated into the initial length growth in a localized area due to the accumulation of cations or anions, followed by lateral filament size expansion afterwards.[10,11] Similar arguments can be made during the RESET processes, where the weakening of magnetization started in area 2 and then moved to area 1. By programming the devices into different resistance states and characterizing the corresponding MFM images, a semi-quantitative relationship between the mean phase value and the resistance value was established and shown in Figure 2f. It can be seen that the mean phase value of the domain can be modulated between 0.1°~0.2° by changing the device resistance between 2.5×10^4 Ω~2×10^2 Ω. Since the phase value ($\Delta\Phi$) obtained in the MFM image is roughly proportional to the intensity of the magnetization of the sample (See discussion in Supplementary Information), Figure 2e indicates that the

Author Manuscript

This article is protected by copyright. All rights reserved.

significant modulation of magnetization (~ 100%) can be obtained in the LFO film through the application of relative low voltages (2-3 volts). By taking the switching current and switching area to be 10^{-3} A and 0.5 μm^2 respectively (extracted from the *I-V* curves and the current map in Figure S9(d)), the current density during the magnetism modulation is estimated to be on the order of 10^5 A/cm^2. We note that a high current density is not necessary to induce the magnetism changes observed here, since ion migration is mainly driven by the electric field and can occur at very low current densities.

The local modulation offered by Li^+ ions de-intercalation/intercalation further leads to interesting domain wall evolutions. **Figures 3**a,b show the *I-V* curves of a device switched between the HRS and the LRS along with the changes of the device resistance. Figure 3c shows the MFM images of an area with apparent magnetism changes. Similar to results in Figure 1, switching of the device from the HRS and the LRS (or from the LRS to the HRS) can reversibly strengthen (or weaken) the overall magnetization in regions with different magnetization directions (Figure S13, Supporting Information), although the magnitude of the magnetization modulation is not spatially uniform due to the localized nature of the ion migration.[5] Furthermore, careful examination of the interface between two neighboring domains with opposite magnetization directions reveals that the non-uniform changes in magnetization leads to reversible domain wall motion during the RS processes. Figure 3c ① shows the initial MFM image with the domain wall center marked by the yellow dashed line. Switching of the device to the LRS resulted in a clear strengthening of the magnetization in the lower left domain (with a downward magnetization direction) and caused the domain wall to shift towards the upper right direction, as marked by the brown dashed line (②). After the subsequent RESET process, the magnetization of the lower left domain was weakened, and the domain wall center shifted back to the lower left side again (③). Further switching of the device

This article is protected by copyright. All rights reserved.

Author Manuscript

between the HRS and LRS can reversibly drive the domain wall motion (④-⑤), though the exact shape of the domain structure may be somewhat different. To more clearly reveal the domain wall evolution, we plot the MFM phase values along the solid line AB (①) during the RS cycles in Figure 3d, which shows that besides the modulation of the intensity, the center of the domain wall (corresponding to the zero-phase point) clearly moves forth and back during RS, over a distance of ~ 100 nm. Additionally, near the center of the domain wall, the polarization also switches between upwards (positive phase) and downwards (negative phase) during the RS process. These effects are more clearly observed by plotting the location of the zero-phase point during the RS process (Figure 3e) and plotting the phase value for a point near the domain wall center (*e.g.* the position marked by the cross in Figure 3c ①) in Figure 3f. These observations are consistent with the picture of domain wall motion driven by controlled Li^+ ions migration (Figure 3g), contrary to the cases in racetrack memory where the domain wall motion is driven by a large in-plane electric current.[48] Significant domain wall motion has also been observed recently in ferromagnetic metal thin films driven by electric fields.[49-51]

In nanoionics-based RS devices, the ion migration can be speeded up exponentially and RS switching can be achieved with nanoseconds.[5] Indeed, **Figure 4**a shows that the LFO devices can be SET and RESET using 300 ns pulses (with higher switching speed possible with higher pulse amplitudes). By taking advantage of changes in magnetization, coupled with resistance changes, these effects can potentially lead to high speed and multifunctional device applications. Here, as an example we show that nanoscale magnetic domains can act as elements for multi-mode storage in which the direction and the intensity of the magnetization of the domains can be independently and switched, and used to store two bits in one physical cell (Figure S14 and S15, Supporting Information). In this case, the upward (downward) magnetization direction is used to represent the

This article is protected by copyright. All rights reserved.

Author Manuscript

first digit of “0” (“1”), and the low (high) intensity of the magnetization is used to represent the second digit of “0” (“1”), respectively. Here switching of the first digit is achieved by changing the direction of the magnetization using an external magnetic field, while the second digit is changed by applying a positive/negative electric pulse to switch the device to the LRS/HRS, which in turn modulates the intensity of the magnetization (high or low).

Figure 4b shows an example that an eight-digit ASCII letter can be stored using four independent magnetic domains in four Pt/LFO/SRO devices. Initially, the devices were all upward-magnetized using a magnetic field (~2000 Oe) and programmed into the HRS with a resistance ~10^4 Ω leading to weak magnetization, corresponding to “00” for all four cells. By switching all four devices to the LRS with a resistance of ~10^2 Ω using a SET pulse (~3 V and 200 ns), strong magnetization is obtained in all four domains leading to the storage of the ASCII letter “U” (“01010101”). Subsequent switching of the magnetization direction and intensity in selected domains leads to the storage of letters “M”, “I”, “C”, and “H” in the same cells, suggesting that reversible, high speed and multilevel magnetic data storage can be obtained in the individual magnetic domains.

In conclusion, we show that reversible, nonvolatile and room temperature control of magnetic properties at the nanoscale can be achieved through electric field controlled ion migration in solid state thin films. Systematic electrical and magnetic measurements reveal the relationship between Li^+ ion migration and nanoscale magnetization modulation during the RS processes in LFO-based devices. Our results show that the magnetization of magnetic domains can be significantly modulated (~100%) by controlling the de-intercalation/intercalation of Li^+ ions, and reversible domain wall motion over a distance of ~100 nm can be achieved locally, thus providing an effective and versatile method to control magnetic properties electrically. Beyond its potential applications in

This article is protected by copyright. All rights reserved.

Author Manuscript

magnetic and spintronic devices, we expect the ability demonstrated here, the nonvolatile and reversible control of a film's chemical composition and physical properties *in-situ* through controlled ion migration, can be used to effectively tailor the properties of a broad range of functional semiconductor materials and lead to the application of new classes of fast, controllable and multifunctional nanoscale devices based on nanoionics.

Author Manuscript

This article is protected by copyright. All rights reserved.

Experimental Section

Sample Preparation: The 60 nm-thick SRO film serving as the bottom electrode was first deposited on a (111) orientated $SrTiO_3$ (STO) substrate using pulsed laser deposition (PLD) at a nominal temperature of 750 °C in an atmosphere of pure oxygen (10 Pa). The LFO film was then deposited on top of the SRO film by PLD at a nominal temperature of 800 °C at an oxygen pressure of 0.1 Pa. The deposition frequency of both the SRO and the LFO films was set to 2 Hz.

*Device fabrication***:** After the LFO film deposition, amorphous silicon oxide (60 nm) was deposited by plasma enhanced chemical vapor deposition (PECVD) method at 200 °C. Afterwards, via structures (2 μm×2 μm) were created by etching through the amorphous silicon oxide layer using reactive ion etching (RIE) using a C4F8/SF6 chemistry to expose the LFO film surface, followed by the deposition of a 60 nm-thick Pt film serving at the top electrode using a DC sputtering method. Additional contact pad structures were subsequently patterned to complete the device structure.

Measurements: The crystal structure was examined with XRD technique (Huber six-circle diffractometer). XPS characterizations were performed using a Kratos Axis Ultra system to analyze the chemical states of the sample with a monochromated Al anode. The electric characterizations were performed using a Keithley semiconductor parameter measurement system. An atomic force microscope (Dimension V, Icon) was used to perform the MFM and C-AFM measurements, and to mechanically remove the Pt electrode before the C-AFM measurements. MFM measurements were performed at a lift height of 30 nm using a magnetic tip coated with Co/Cr thin film (MESP, Bruker). Before the MFM measurements, a

Author Manuscript

This article is protected by copyright. All rights reserved.

magnetic field of ~2000 Oe was used to magnetize the tip's magnetization direction downward. To remove the Pt electrode, a silicon probe with a cantilever spring constant of 42 N/m (Bruker, TESPA-V2) was used to mechanically scrape the Pt electrode. The contact force between the probe and the Pt electrode was set to ~1 μN during the process. During the C-AFM measurements, a conducting cantilever coated with Pt/Ir (PPP-CONTPt, Nanosensors) was used in the contact mode, and the contact force was set to ~30 nN.

Supporting Information

Supporting Information is available from the Wiley Online Library or from the author.

Acknowledgements

The authors would like to thank Dr. Bing Chen for useful discussion. This work was supported in part by the AFOSR through MURI grant FA9550-12-1-0038, the State Key Project of Fundamental Research of China (973 Program, 2012CB933004), National Natural Science Foundation of China (51525103, 11474295, 61328402) and Ningbo Science and Technology Innovation Team (2015B11001).

Author Manuscript

This article is protected by copyright. All rights reserved.

References

[1] J. Maier. *Nat. Mater.* **2005,** *4*, 805-815.
[2] J. Maier. *Chem. Mater.* **2014,** *26*, 348-360.
[3] R. Waser, M. Aono. *Nat. Mater.* **2007,** *6*, 833-840.
[4] A. L. Despotuli, A. V. Andreeva. *Nanotechnologies in Russia* **2010,** *5*, 506-520.
[5] R. Waser, R. Dittmann, G. Staikov, K. Szot. *Adv. Mater.* **2009,** 2632-2663.
[6] J. J. Yang, D. B. Strukov, D. R. Stewart. *Nat. Nanotechnol.* **2013,** *8*, 13-24.
[7] Y. Yang, W. Lu. *Nanoscale* **2013,** *5*, 10076-10092.
[8] Y. Yang, P. Gao, S. Gaba, T. Chang, X. Pan, W. Lu. *Nat. Commun.* **2012,** *3*, 732.
[9] D.-H. Kwon, K. M. Kim, J. H. Jang, J. M. Jeon, M. H. Lee, G. H. Kim, X.-S. Li, G.-S. Park, B. Lee, S. Han, M. Kim, C. S. Hwang. *Nat. Nanotechnol.* **2010,** *5*, 148-153.
[10] D. Ielmini. *IEEE Trans Electron* **2011,** *58*, 4309-4317.
[11] S. Kim, S. Choi, W. Lu. *ACS Nano* **2014,** *8*, 2369-2376.
[12] A. Emboras, I. Goykhman, B. Desiatov, N. Mazurski, L. Stern, J. Shappir, U. Levy. *Nano Lett.* **2013,** *13*, 6151-6155.
[13] A. S. Arico, P. Bruce, B. Scrosati, J.-M. Tarascon, W. van Schalkwijk. *Nat. Mater.* **2005,** *4*, 366-377.
[14] Y. Huai. *AAPPS Bulletin* **2008,** *18*, 33-40.
[15] A. D. Kent, D. C. Worledge. *Nat. Nanotechnol.* **2015,** *10*, 187-191.
[16] F. Matsukura, Y. Tokura, H. Ohno. *Nat. Nanotechnol.* **2015,** *10*, 209-220.
[17] S. Parkin, S.-H. Yang. *Nat. Nanotechnol.* **2015,** *10*, 195-198.
[18] C. Chappert, A. Fert, F. N. Van Dau. *Nat. Mater.* **2007,** *6*, 813-823.
[19] H. Ohno, D. Chiba, F. Matsukura, T. Omiya, E. Abe, T. Dietl, Y. Ohno, K. Ohtani. *Nature* **2000,** *408*, *944-946*.
[20] D. Chiba, M. Yamanouchi, F. Matsukura, H. Ohno. *Science* **2003,** *301*, 943-945.
[21] T. Maruyama, Y. Shiota, T. Nozaki, K. Ohta, N. Toda, M. Mizuguchi, A. Tulapurkar, T. Shinjo, M. Shiraishi, S. Mizukami. *Nat. Nanotechnol.* **2009,** *4*, 158-161.
[22] M. Endo, S. Kanai, S. Ikeda, F. Matsukura, H. Ohno. *Appl. Phys. Lett.* **2010,** *96*, 212503.
[23] Y.-H. Chu, L. W. Martin, M. B. Holcomb, M. Gajek, S.-J. Han, Q. He, N. Balke, C.-H. Yang, D. Lee, W. Hu. *Nat. Mater.* **2008,** *7*, 478-482.
[24] M. Ghidini, R. Pellicelli, J. L. Prieto, X. Moya, J. Soussi, J. Briscoe, S. Dunn, N. D. Mathur. *Nat. Commun.* **2013,** *4*, 1453.
[25] V. Skumryev, V. Laukhin, I. Fina, X. Martí, F. Sánchez, M. Gospodinov, J. Fontcuberta. *Phys. Rev. Lett.* **2011,** *106*, 057206.
[26] Y. Tokunaga, Y. Taguchi, T. Arima, Y. Tokura. *Nat. Phys.* **2012,** *8*, 838-844.

Author Manuscript

This article is protected by copyright. All rights reserved.

[27] Y. Takahashi, R. Shimano, Y. Kaneko, H. Murakawa, Y. Tokura. *Nat. Phys.* **2012,** *8*, 121-125.
[28] S. Kibayashi, Y. Takahashi,, S. Seki, Y. Tokura. *Nat. Commun.* **2014,** *5*, 4583.
[29] W.-G. Wang, M. Li, S. Hageman, C. L. Chien. *Nat. Mater.* **2012,** *11*, 64-68.
[30] Y. W. Yin, J. D. Burton, Y. M. Kim, A. Y. Borisevich, S. J. Pennycook, S. M. Yang, T. W. Noh, A. Gruverman, X. G. Li, E. Y. Tsymbal, Q. Li. *Nat. Mater.* **2013,** *12*, 397-402.
[31] V. Garcia, M. Bibes, L. Bocher, S. Valencia, F. Kronast, A. Crassous, X. Moya, S. Enouz-Vedrenne, A. Gloter, D. Imhoff, C. Deranlot, N. D. Mathur, S. Fusil, K. Bouzehouane, A. Barthélémy. *Science* **2010,** *327*, 1106-1110.
[32] S. Dasgupta, B. Das, M. Knapp, R. A. Brand, H. Ehrenberg, R. Kruk, H. Hahn. *Adv. Mater.* **2014,** *26*, 4639-4644.
[33] X. Chen, X. Zhu, W. Xiao, G. Liu, Y. P. Feng, J. Ding, R.-W. Li. *ACS Nano* **2015,** *9*, 4210-4218.
[34] U. Bauer, L. Yao, A. J. Tan, P. Agrawal, S. Emori, H. L. Tuller, S. van Dijken, G. S. D. Beach. *Nat. Mater.* **2015,** *14*, 174-181.
[35] X. Wang, L. Gao, L. Li, H. Zheng, Z. Zhang, W. Yu, Y. Qian. *Nanotechnology* **2005,** *16*, 2677.
[36] J. Dormann, A. Tomas, M. Nogues. *Phys. Status. Solidi. A* **1983,** *77*, 611-618.
[37] D. S. Mathew, R.-S. Juang. *Chem. Eng. J.* **2007,** *129*, 51-65.
[38] R. Gunning, K. Rode, S. R. Sofin, M. Venkatesan, J. Coey, I. V. Shvets, J. G. Lunney. *Appl. Surf. Sci.* **2009,** *255*, 5245-5247.
[39] U. Celano, L. Goux, A. Belmonte, K. Opsomer, A. Franquet, A. Schulze, C. Detavernier, O. Richard, H. Bender, M. Jurczak, W. Vandervorst. *Nano Lett.* **2014,** *14*, 2401-2406.
[40] S. Takai, K. Yoshioka, H. Iikura, M. Matsubayashi, T. Yao, T. Esaka. *Solid State Ionics* 2014, *256*, 93-96.
[41] A. Moradpour, O. Schneegans, S. Franger, A. Revcolevschi, R. Salot, P. Auban-Senzier, C. Pasquier, E. Svoukis, J. Giapintzakis, O. Dragos, V.-C. Ciomaga, P. Chrétien. *Adv. Mater.* **2011,** *23*, 4141-4145.
[42] V. H. Mai, A. Moradpour, P. A. Senzier, C. Pasquier, K. Wang, M. J. Rozenberg, J. Giapintzakis, C. N. Mihailescu, C. M. Orfanidou, E. Svoukis, A. Breza, C. B. Lioutas, S. Franger, A. Revcolevschi, T. Maroutian, P. Lecoeur, P. Aubert, G. Agnus, R. Salot, P. A. Albouy, R. Weil, D. Alamarguy, K. March, F. Jomard, P. Chrétien, O. Schneegans. *Sci. Rep.* **2015,** *5*, 7761.
[43] X. Zhu, C. S. Ong, X. Xu, B. Hu, J. Shang, H. Yang, S. Katlakunta, Y. Liu, X. Chen, L. Pan, J. Ding, R.-W. Li. *Sci. Rep.* **2013,** *3*, 1084.
[44] W. Hu, N. Qin, G. Wu, Y. Lin, S. Li, D. Bao. *J. Am. Chem. Soc.* **2012,** *134*, 14658-14661.

Author Manuscript

This article is protected by copyright. All rights reserved.

[45] Y. Xia, W. He, L. Chen, X. Meng, Z. Liu. *Appl. Phys. Lett.* **2007,** *90*, 022907.
[46] S. H. Chang, N. Danilovic, K.-C. Chang, R. Subbaraman, A. P. Paulikas, D. D. Fong, M. J. Highland, P. M. Baldo, V. R. Stamenkovic, J. W. Freeland, J. A. Eastman, N. M. Markovic. *Nat. Commun.* **2014,** *5*, 4191.
[47] P. Balaya, H. Li, L. Kienle, J. Maier. *Adv. Funct. Mater.* **2003,** *13*, 621-625.
[48] S. S. P. Parkin, M. Hayashi, L. Thomas. *Science* **2008,** *320*, 190-194.
[49] T. Dohi, S. Kanai, A. Okada, F. Matsukura, H. Ohno. arXiv:1603.08280.
[50] H. Kakizakai, F. Ando, T. Koyama, K. Yamada, M. Kawaguch, S. Kim, K.-J. Kim, T. Moriyama, D. Chiba, T. Ono. *Appl. Phys. Express* **2016,** *9*, 063004.
[51] F. Ando, H. Kakizakai, T. Koyama, K. Yamada, M. Kawaguchi, S. Kim, K-J. Kim, T. Moriyama, D. Chiba, and T. Ono. arXiv:1604.02770.

Author Manuscript

This article is protected by copyright. All rights reserved.

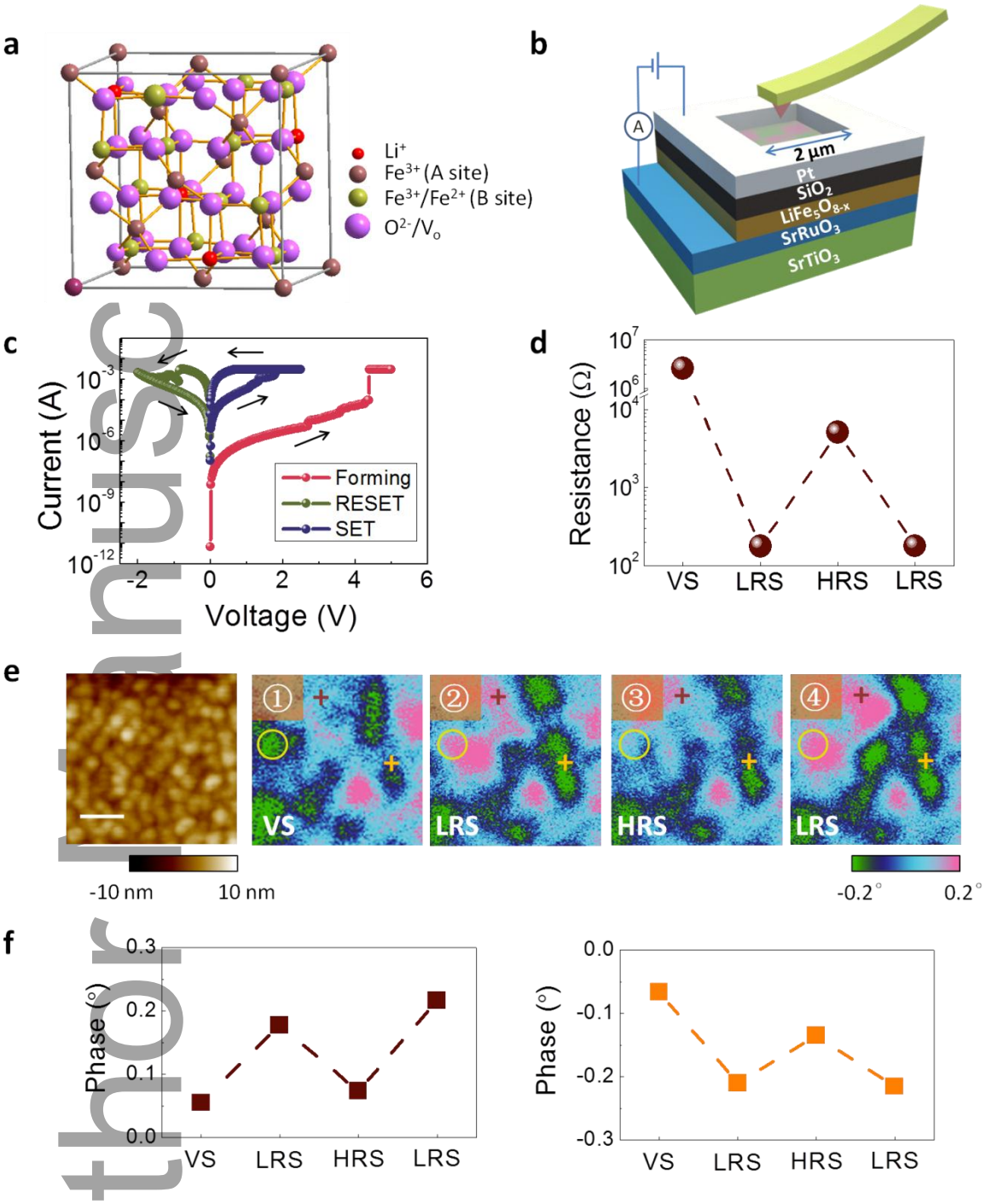

Figure 1 Reversible modulation of magnetic domain properties in Pt/LFO/SRO devices. a) The inverse spinel structured $LiFe_5O_8$ unit cell. b) Schematic of the measurement setup. After

This article is protected by copyright. All rights reserved.

programming the Pt/LFO/SRO device (defined by the via structure), the MFM images were obtained without the bias voltage. c) Current-Voltage (*I-V*) Characteristics of the Pt/LFO/SRO device during the RS process, showing the Forming, RESET and SET processes. d) Device resistance programmed in different states. e) Morphology and corresponding MFM images of the device at different resistance states in (d). The marked locations highlight the areas where the magnetization has changed. Scale bar: 300 nm. f) MFM phase at different resistance states in (d), measured at the two locations marked by the brown and yellow crosses in the MFM images in (e).

Author Manuscript

This article is protected by copyright. All rights reserved.

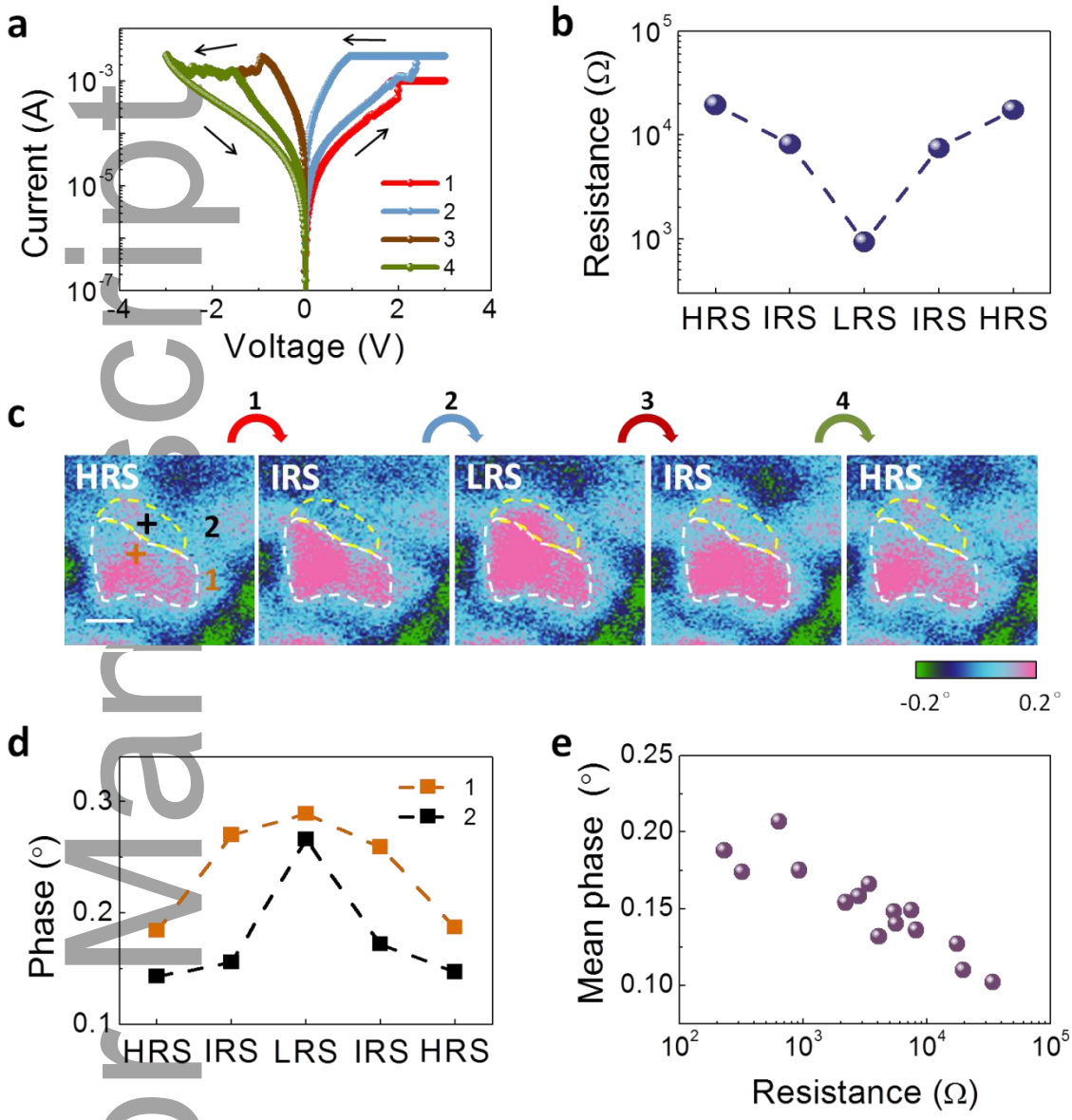

Figure 2 Correlation of Li^+ ion migration with magnetization modulation during RS processes. a) *I-V* characteristics of the Pt/LFO/SRO device during consecutive RS processes. b) Measured device resistance at different states. c) MFM images of an area with a dominant upward domain at different resistance states in (b). Scale bar: 200 nm. d) MFM phase value measured at different resistances in (b), measured at the two locations marked by the brown and black crosses in area 1 and 2 in (c). e) Correlation of the mean phase value measured from the whole domain area (area 1 plus area 2) and the device resistance.

This article is protected by copyright. All rights reserved.

Author Manuscript

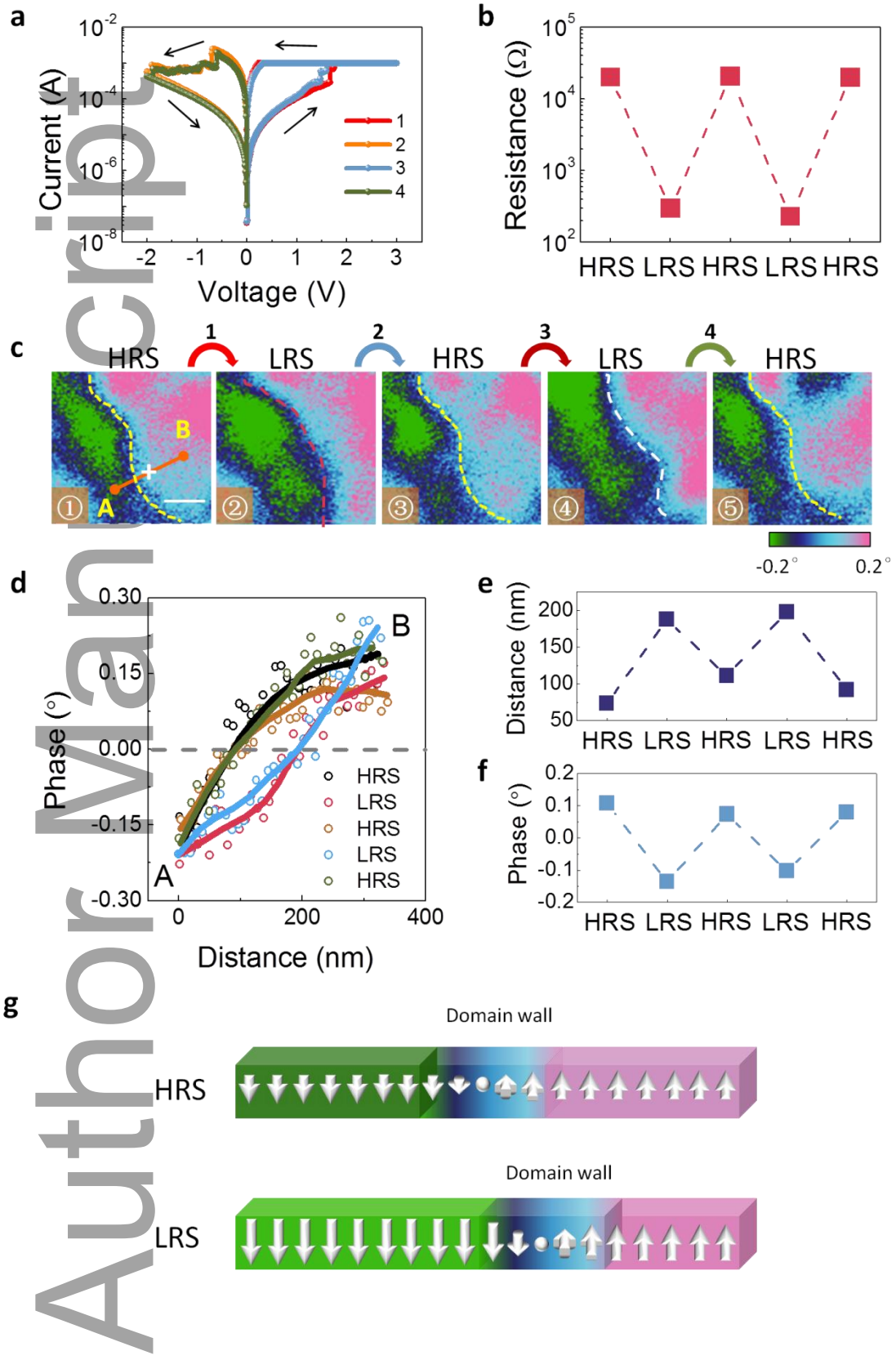

Author Manuscript

This article is protected by copyright. All rights reserved.

Figure 3 Controlled magnetic domain wall motion in the LFO thin film. a) *I-V* characteristics of the Pt/LFO/SRO device during two consecutive RS processes. b) Measured device resistance at different states. c) MFM images of an area with apparent magnetization changes, measured at different resistance states in (b). The dashed line in each MFM image marked the position of the domain wall center. Scale bar: 200 nm. d) Measured MFM phase values along line AB in the MFM images in (c)**,** at the different resistance states. e) Location of the zero-phase point obtained from (c) at different resistance states. f) Measured phase value at different resistance states, measured at the location marked by the yellow cross near the domain wall center shown in (c). g) Schematics showing possible magnetic domain wall motion when the device was switched between the HRS and the LRS.

Author Manuscript

This article is protected by copyright. All rights reserved.

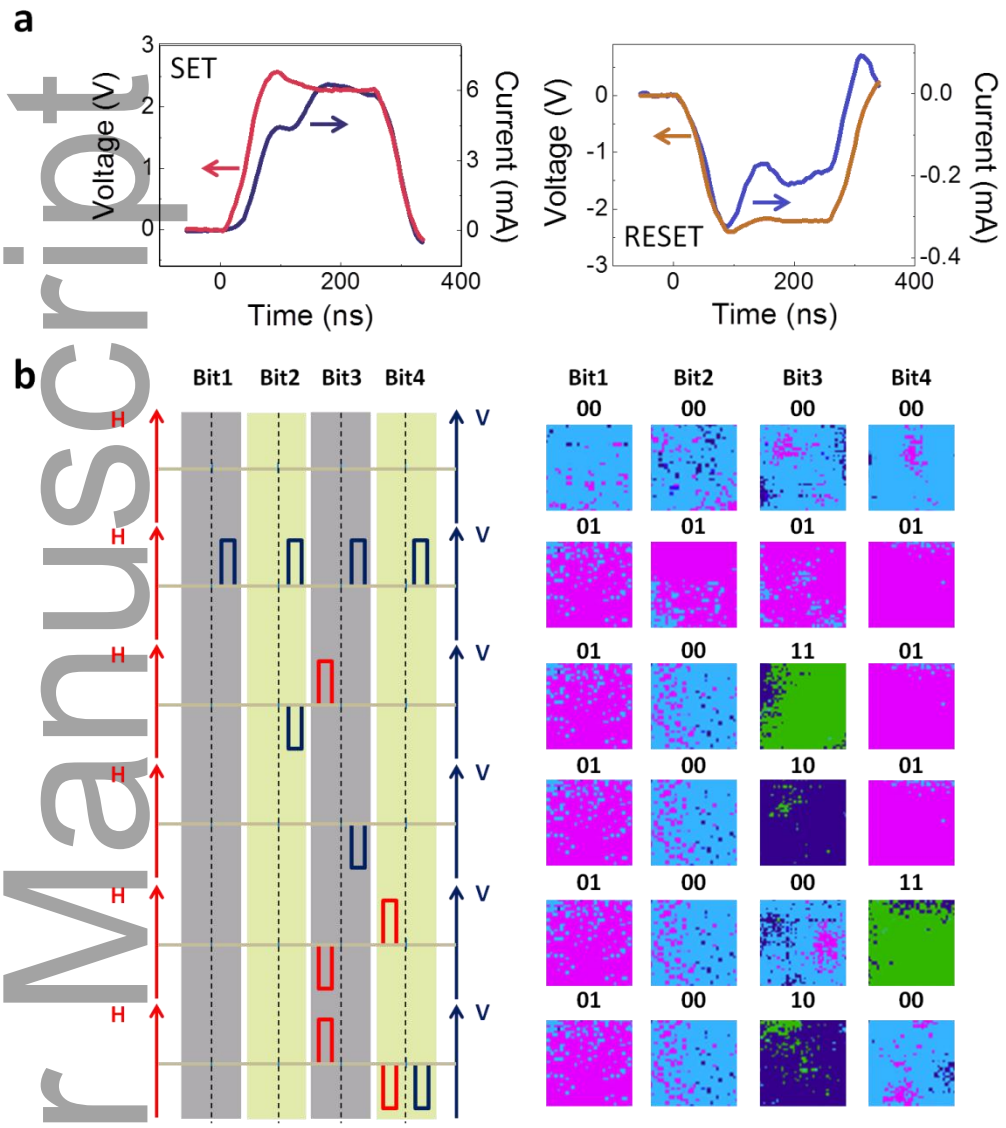

Figure 4 High speed, reversible and multilevel data storage based on magnetic domains. a) Time dependent transient switching characteristics in a Pt/LFO/SRO device during the SET and RESET processes. The amplitude and width of the SET and RESET pulses are ±2.2 V and 300 ns. b) Magnetic field and electric pulse sequence used to program the domains (left) and the stored data read out using MFM measurements (right). Four domains (size 200 nm×200 nm) from four individual devices were used in this measurement. Five letters corresponding to American

Author Manuscript

This article is protected by copyright. All rights reserved.

Standard Code (ASCII) code “U”, “M”, “I”, “C” and “H” were sequentially programmed into the domains.

Author Manuscript

This article is protected by copyright. All rights reserved.

The table of contents entry

Author Manuscript

Direct, nonvolatile and reversible control of nanomagnetism in solid-state ferromagnetic thin films is achieved by controlling the chemical composition of the film through field-driven ion redistribution. The electric field driven de-intercalation/intercalation of lithium ions can result in ~100% modulation of the magnetization and drives domain wall motion over ~100 nm. High speed and multilevel magnetic information storage is further demonstrated.

Keyword: Nanomagnetism, ion migration, resistive switching, intensity of the magnetization, domain wall

*Xiaojian Zhu, Jiantao Zhou, Lin Chen, Shanshan Guo, Gang Liu, Run-Wei Li, and Wei D. Lu**

In-situ Nanoscale Electric Field Control of Magnetism by Nanoionics

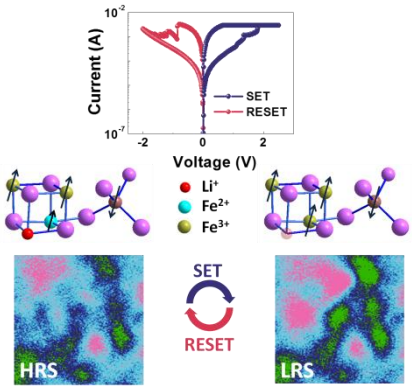

This article is protected by copyright. All rights reserved.